Electronic Supplementary Information (ESI)

Stringed "tube on cube" nanohybrids as compact cathode matrix for high-loading and lean-electrolyte lithium-sulfur batteries

Gaoran Li,[‡a] Wen Lei,[‡b] Dan Luo,[a] Yaping Deng,[a] Zhiping Deng,[b] Deli Wang,[*b] Aiping Yu,[a] Zhongwei Chen[*a]

[a]Department of Chemical Engineering, Waterloo Institute for Nanotechnology, Waterloo Institute for Sustainable Energy, University of Waterloo, Waterloo, Ontario N2L 3G1, Canada

[b]Key laboratory of Material Chemistry for Energy Conversion and Storage, Hubei Key Laboratory of Material Chemistry and Service Failure, School of Chemistry and Chemical Engineering, Huazhong University of Science and Technology, Wuhan 430074, P. R. China

‡These authors contribute equally to this work.

*corresponding authors: zhwchen@uwaterloo.ca; wangdl81125@hust.edu.cn

1. Experimental

Synthesis ZIF-67 cube. 580 mg of $Co(NO_3)_2 \cdot 6H_2O$ was dissolved in 20 mL deionized water containing 30 mg CTAB as surfactant. Afterwards, the obtained solution was rapidly added into 140 mL aqueous solution with 9.08 g of 2-methylimidazole and vigorously stirred at room temperature for 60 min. The purple precipitate was collected by centrifugation and washed with ethanol and deionized water repeatedly.

Synthesis of CPZ composite fabric. 0.2 g of the as-synthesized ZIF-67 powder was dispersed in 7.38 mL of dimethylformamide (DMF) solvent via sonication for 2 h, which was followed by the addition of different amounts of polyacrylonitrile (PAN, average MW 15 w). The mixture was stirred over 24 h to form a homogeneous purple suspension. Then, the mixture solution was loaded into a syringe (10 mL) with a stainless-steel nozzle, which was connected to a high-voltage power supply. The high voltage, feeding rate, temperature and distance between the anode and cathode are controlled at 19 kV, 1.1 mL h^{-1}, 25 °C and 18 cm, respectively. The electrospun PZ composite fabric was then vacuum dried at 80 °C overnight, and subsequently carbonized at 900 °C with a ramping rate of 2 °C min^{-1} under the Ar atmosphere. The weight ratio of PAN to ZIF is varied from 10:1, 5:1, 3:1 to 2:1.

Synthesis of CPZC composite fabric. The CPZC fabric was obtained by applying a Chemical Vapor Deposition (CVD) technology process following the thermostatic carbonization process of PZ composite fabric at 900 ºC by using ethylenediamine as the gas precursor without any additional catalyst. The ethylenediamine gas velocity was controlled at 3 mL h^{-1} for CNT growth, while the CVD time was controlled by varying the amount of ethylenediamine (1 mL, 2 mL and 3 mL). The optimized CPZC fabric (PAN to ZIF ratio of 2:1 and ethylenediamine dosage of 3 mL) shows a density around 0.28 g cm^{-3}.

Fabrication of sulfur electrodes. Sulfur composites (S@CP, S@CPZ, and S@CPZC) were prepared by adding the 0.5 M S/CS_2 solution into the obtained carbonaceous fabrics, which were dried under 60 ºC for 6 h and further thermally treated at 155 ºC for 12 h. The areal sulfur loading was around 1.5 mg cm^{-2} for regular electrodes, while higher sulfur loadings of 2.8, 5.1, 9.2, and 13.5 mg cm^{-2} were also prepared for higher energy density.

Structural characterization. SEM (LEO FESEM 1530) and TEM (JEOL2010F TEM/STEM) were performed to investigate the morphologies and microstructures of the obtained samples. The XRD patterns were recorded by MiniFlex 600 Rigaku diffractometer. The pore structure was studied by nitrogen sorption (ASAP 2020 micromeritics) based on Brunauer-Emmett-Teller theory. The Raman spectrometry was performed with a DXR Raman microscope. XPS spectra were collected by Thermo Scientific K-Alpha spectrometer to study the surface chemistry of the obtained samples. The UV-vis spectra were collected by Thermo Scientific GENESYS 10S spectrophotometer. The TGA study was performed by TA instruments Q500 at a heating rate of 5 °C min^{-1} under N_2 atmosphere.

Electrochemical characterization. The CR2032 coin cells were assembled by using sulfur composite electrode as cathode, Celgard 2325 membrane as separator, and lithium foil as anode in Ar-filled glove box with moisture and oxygen level lower than 0.5 ppm. The electrolyte contains 1M lithium bis(trifluoromethane) sulfonamide (LiTFSI) in a binary solvent of dimethoxymethane/1,3-dioxolane (DME/DOL, 1:1 by volume) with 2 wt.% $LiNO_3$ as additive. The electrolyte addition is 12 mL g^{-1}_S for regular cells, while lower E/S ratios of 6, 4.5, and 3 mL g^{-1}_S were also applied to pursue higher energy density. Galvanostatic and multi-rate cycling were performed on a LAND. The current density and specific capacity are calculated based on the mass of sulfur. The CV data was recorded by a Gamry 5000E workstation within the voltage range of 1.8-2.6 V (vs. Li^+/Li) at a scanning rate of 0.1 mV s^{-1}. The EIS study was also performed by Gamry 5000E workstation in frequency range of 0.1 Hz to 100k Hz with an amplitude of 5 mV. The symmetrical cells were assembled by using the obtained fabric as both cathode and anode with the electrolyte containing 0.5 M Li_2S_6. The CV curves of the symmetrical cells were recorded at a scanning rate of 50 mV s^{-1} in the potential range of -0.6 to 0.6 V.

2. Figures and Tables

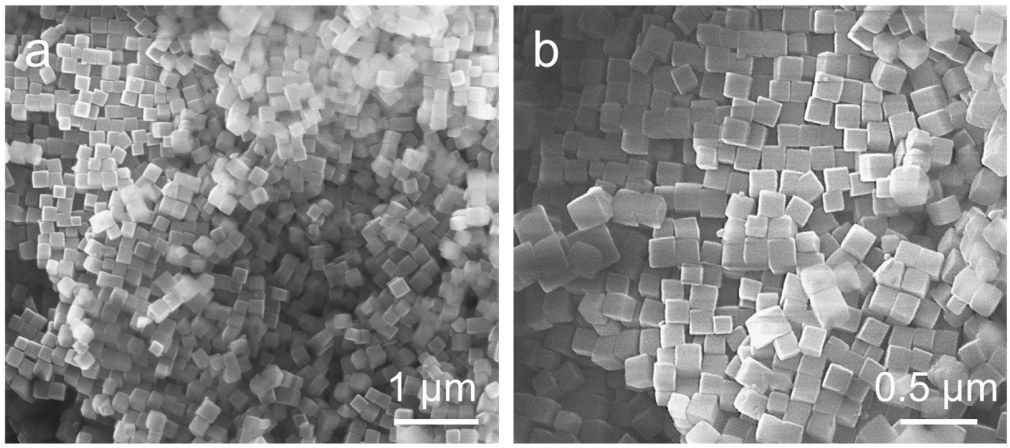

Figure S1. SEM images of the obtained ZIF-67 nanocubes.

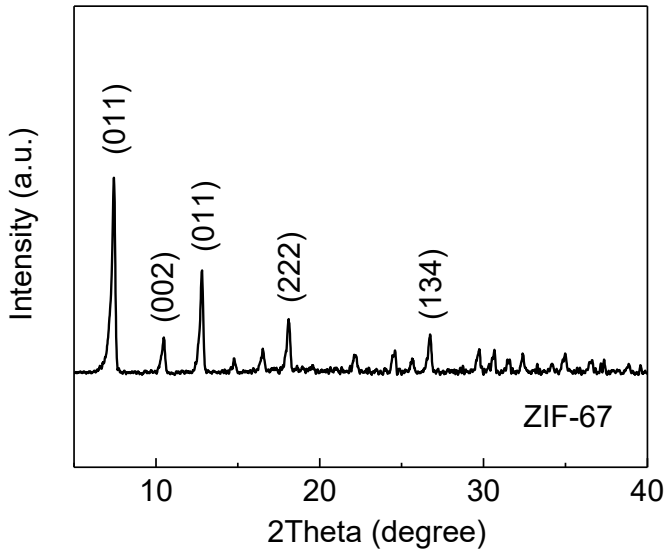

Figure S2. XRD pattern of the obtained ZIF-67 nanocubes.

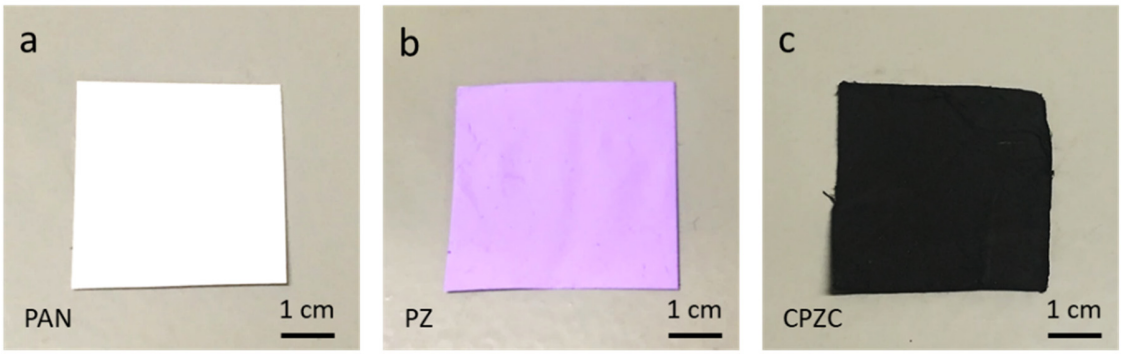

Figure S3. Optical photographs of the obtained PAN (a), PZ (b), and CPZC (c) fabrics.

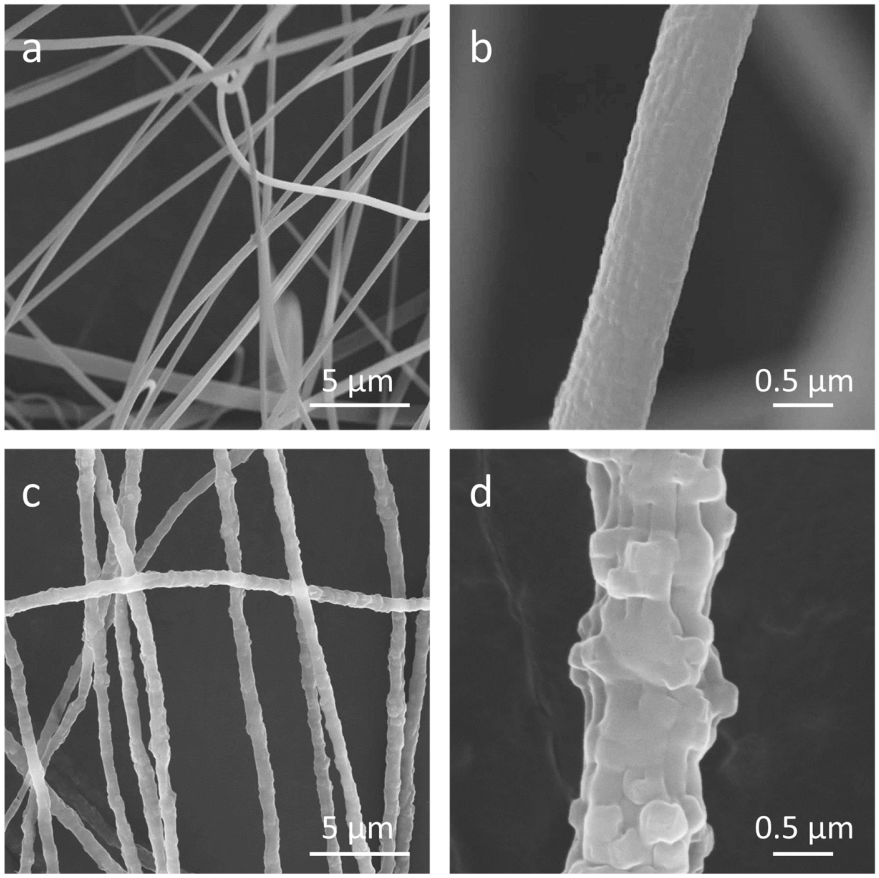

Figure S4 SEM images of PAN (a, b) and PZ composite (c, d) fibers.

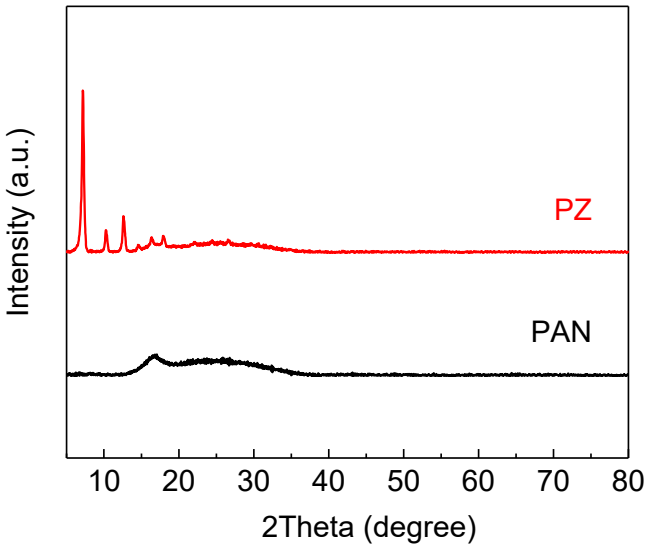

Figure S5. XRD patterns of the obtained PAN and PZ composite fibers.

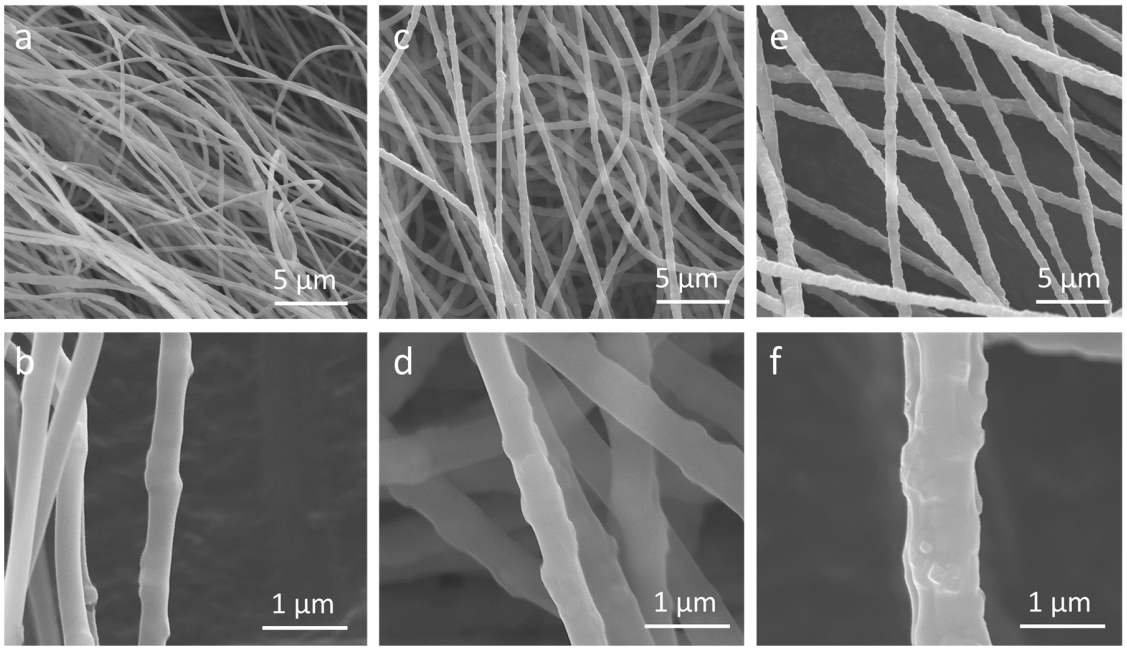

Figure S6. SEM images of PZ composite fiber with PAN to ZIF ratio of 10:1 (a, b), 5:1 (c, d), and 3:1 (e, f).

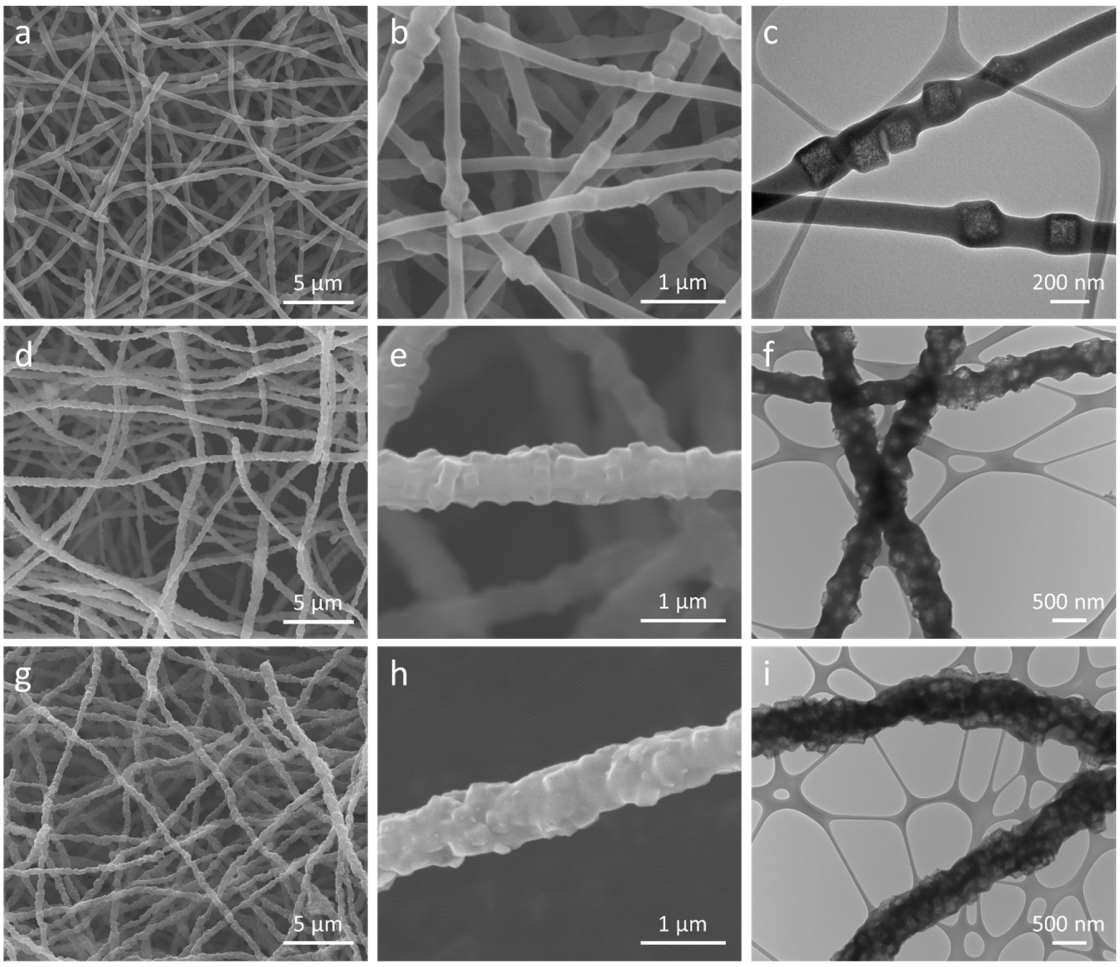

Figure S7. SEM and TEM images of CPZ composite fibers with PAN to ZIF ratio of 10:1 (a-c), 5:1 (d-f), and 3:1 (g-i).

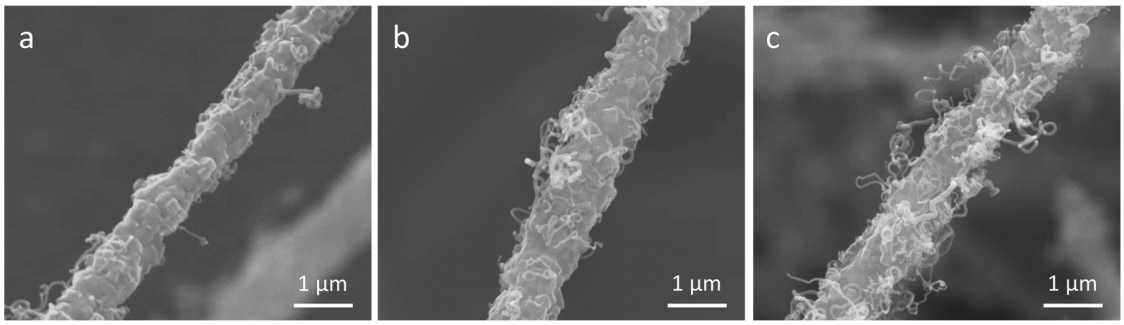

Figure S8. SEM images of CPZC composite fibers with different EDA usage of 1 mL (a), 2 mL (b), and 3 mL (c).

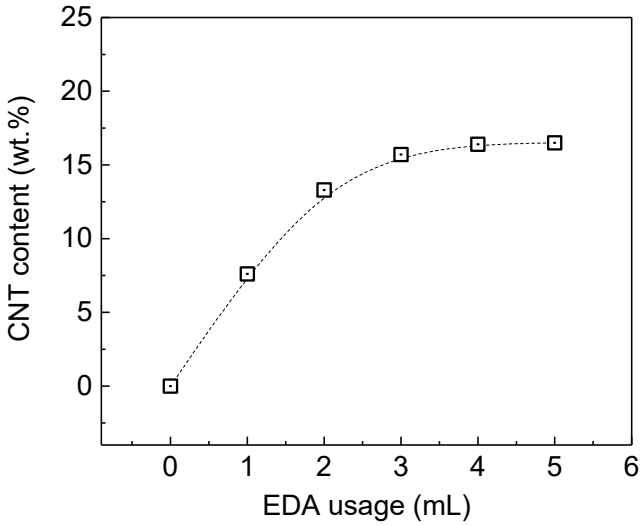

Figure S9. The increase of CNT content in CPZC composite fabric upon the EDA usage in the CVD process. The CNT weight content is calculated based on the mass variation before and after CVD process.

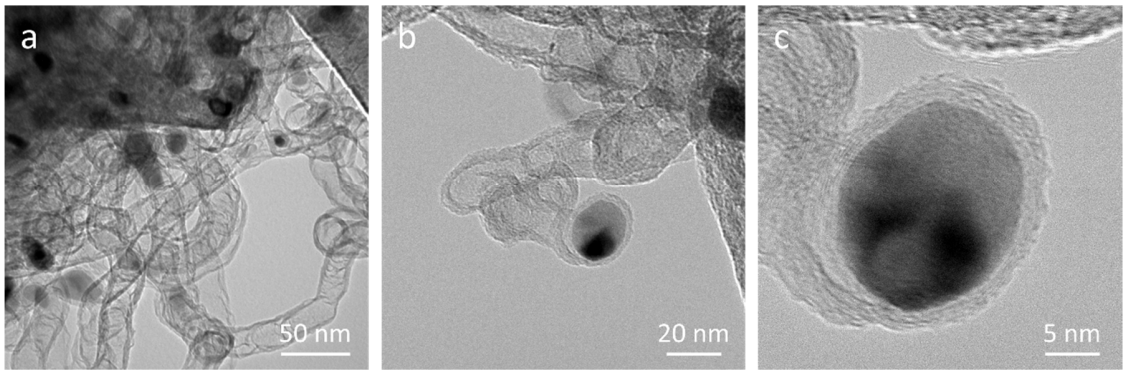

Figure S10. High-resolution TEM images showing the bamboo-like morphology and the highly graphitized carbon walls of the CNTs in CPZC composite fabric.

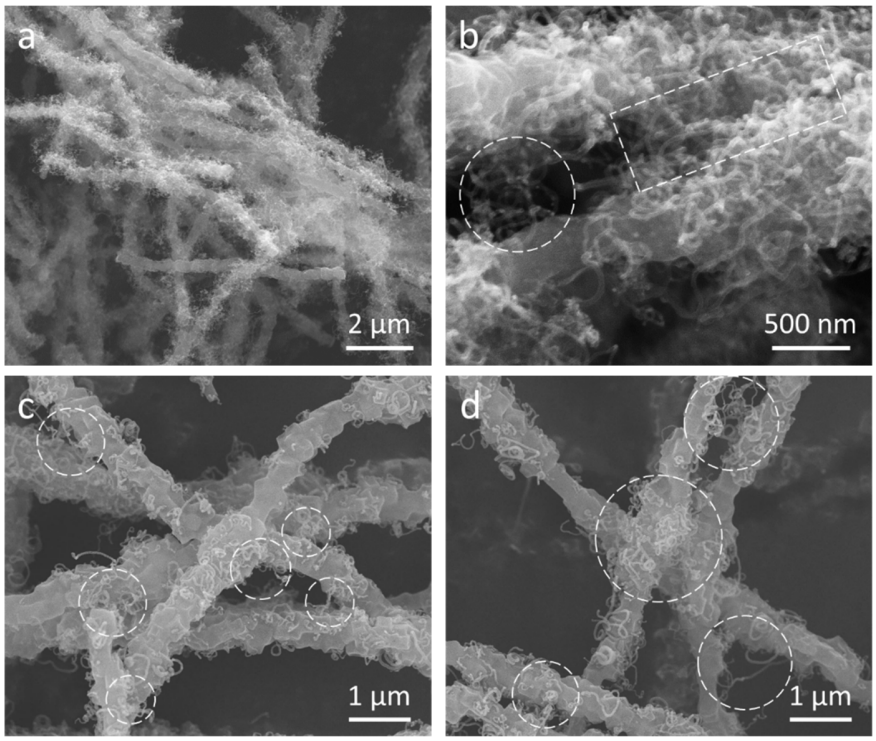

Figure S11. SEM images showing the CNTs intertwining at the junctions of CPZC fibers.

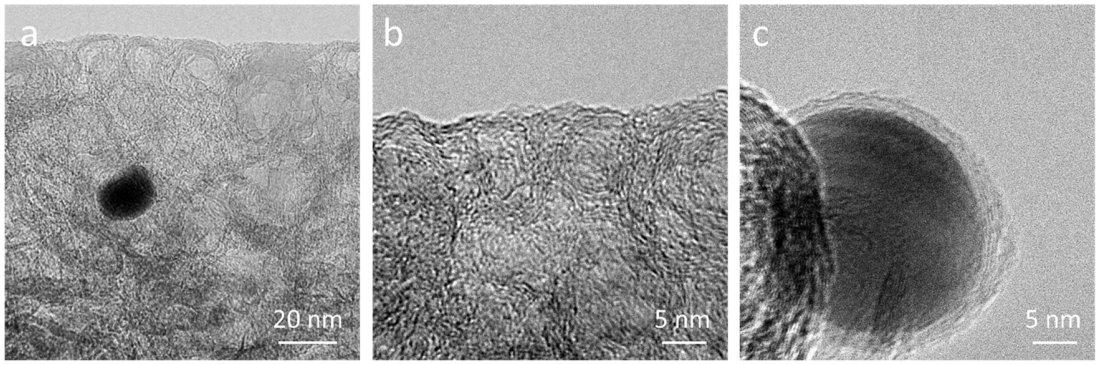

Figure S12. TEM images showing the high graphitized carbon in CPZ composite fabric.

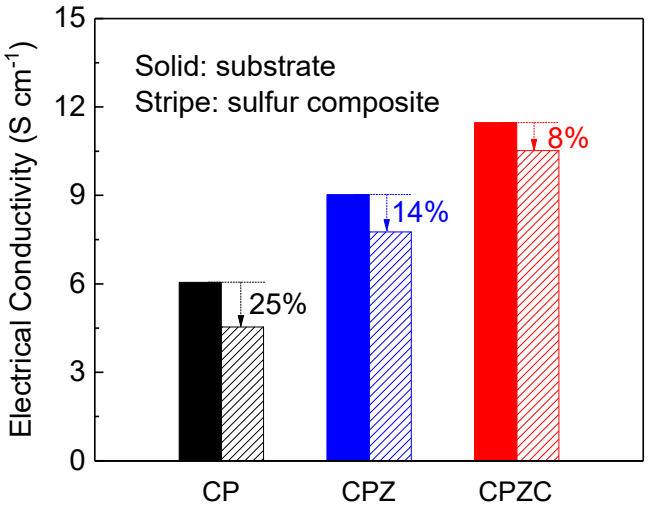

Figure S13. Electrical conductivities of the obtained CP, CPZ, and CPZC fabrics as well as their according sulfur composites.

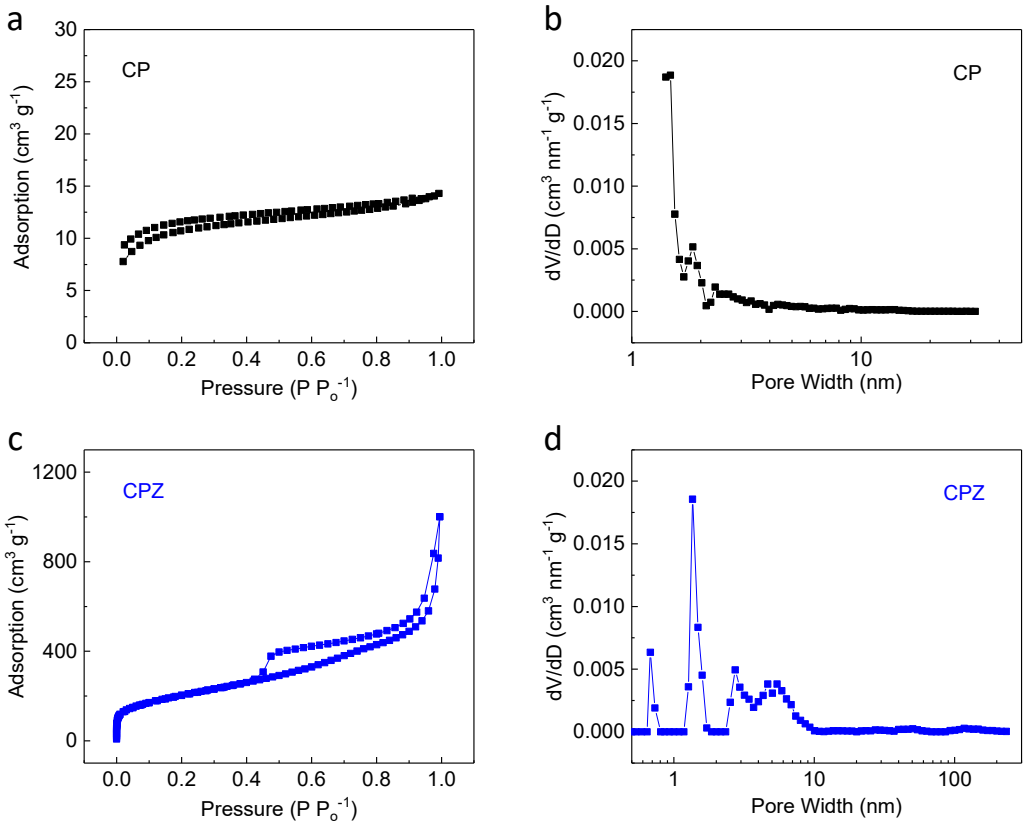

Figure S14. Isotherm curves and pore distributions of CP (a, b) and CPZ (c, d) fabrics.

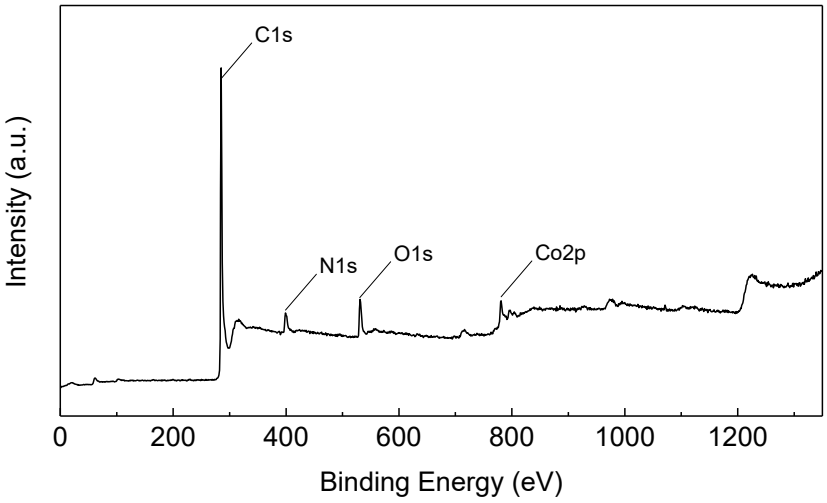

Figure S15. XPS survey spectrum of the obtained CPZC fabric.

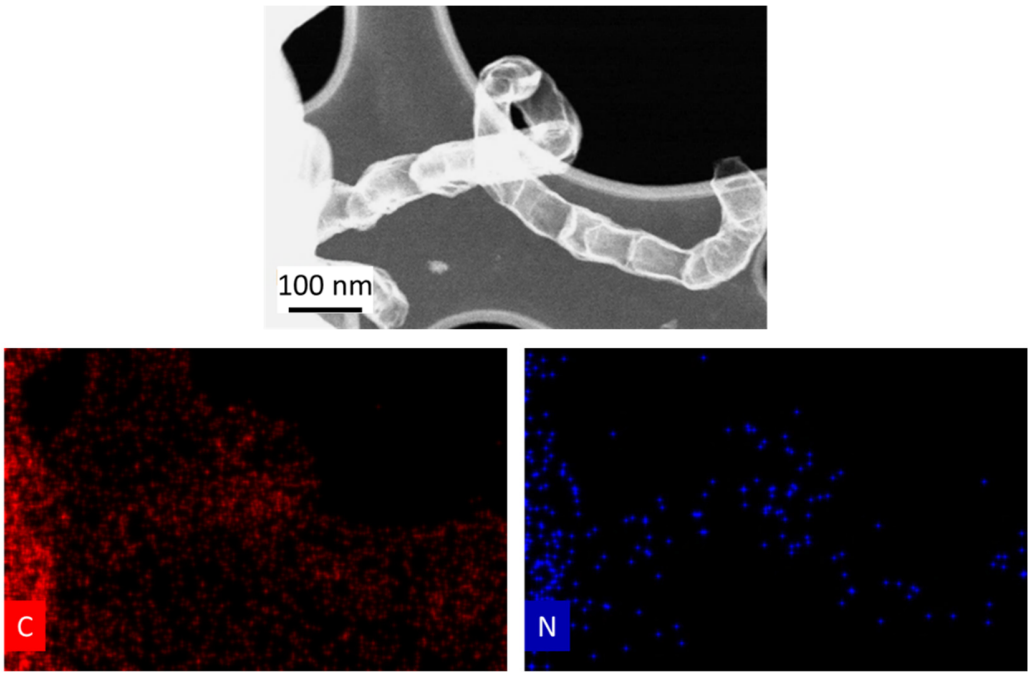

Figure S16. Element mapping of the CNTs grown in the CPZC composite fabric.

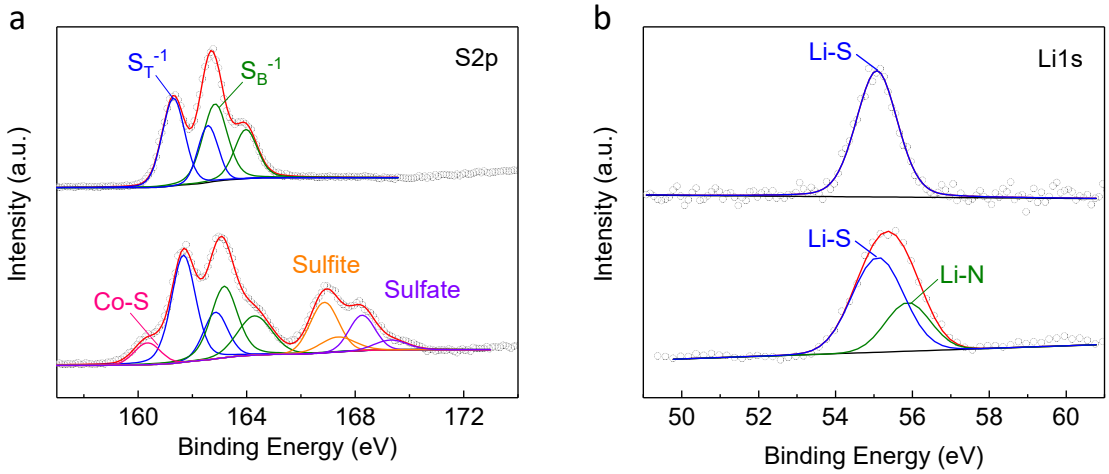

Figure S17. XPS spectra of S2p (a) and Li1s (b) for polysulfide adsorbed by CPZC.

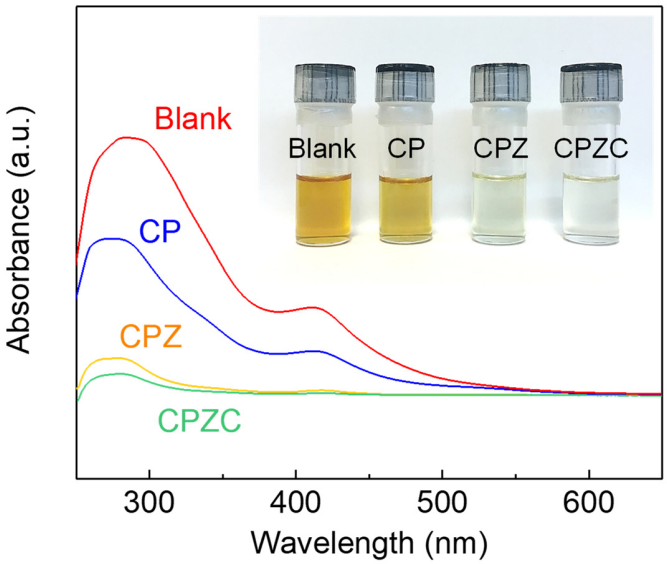

Figure S18. The UV-vis spectra and optical images of polysulfide solution after adsorption by CP, CPZ, and CPZC fabrics. It should be noted that the solvent selection could affect the adsorption behavior since the polysulfide status varies in different solvent system.[1-3] However, such effect does not affect the conclusion here that the CPZC is the most polysulfide adsorptive, because the comparison was conducted in the same solvent system. The purpose of such solvent selection, namely, the DME/DOL binary system, is to simulate the real battery operational environment as far as possible.

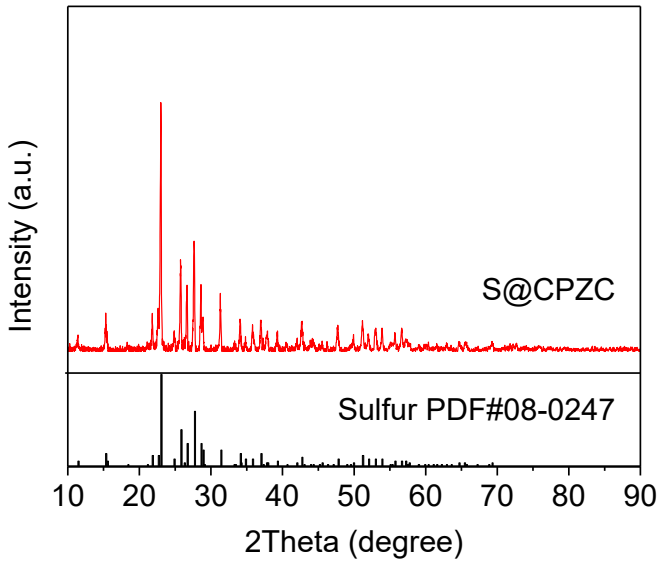

Figure S19. XRD pattern of the S@CPZC composite.

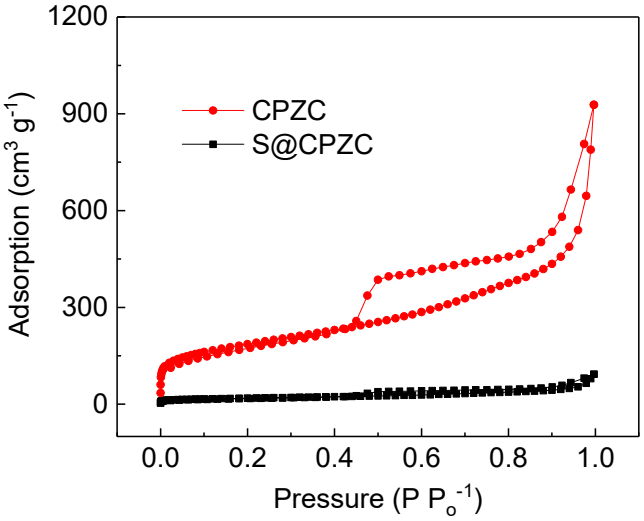

Figure S20. N_2 adsorption/desorption isotherm of CPZC before and after sulfur loading.

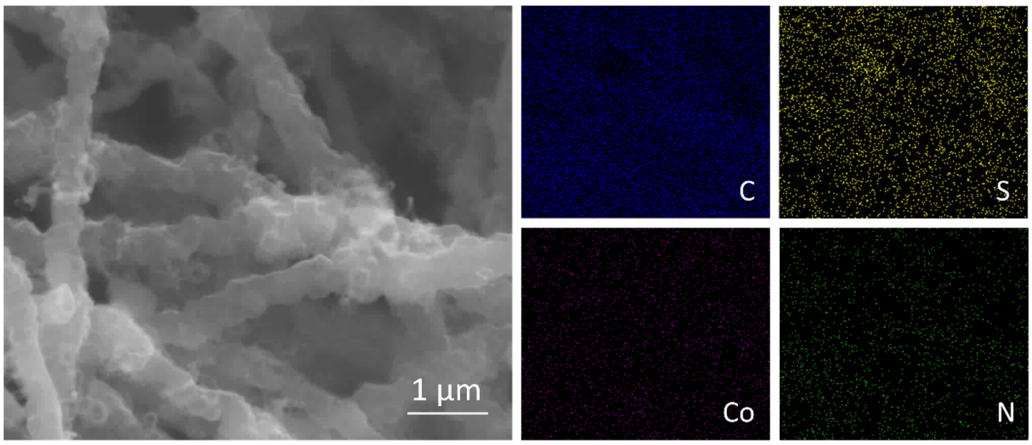

Figure S21. Element mapping of S@CPZC composite.

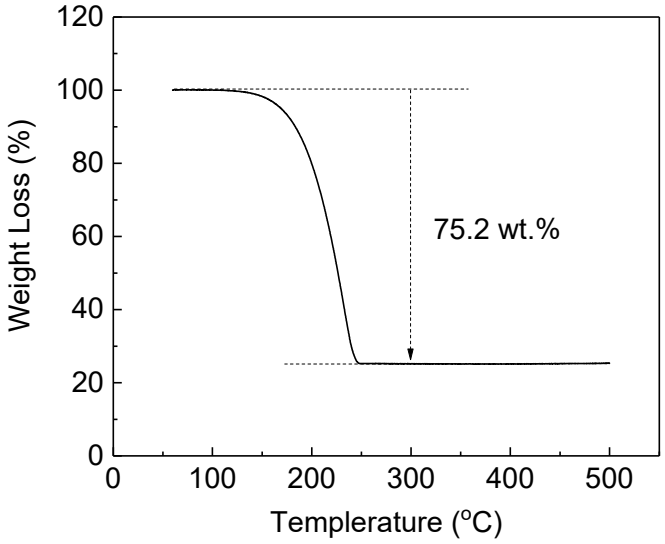

Figure S22. TGA analysis of S@CPZC composite.

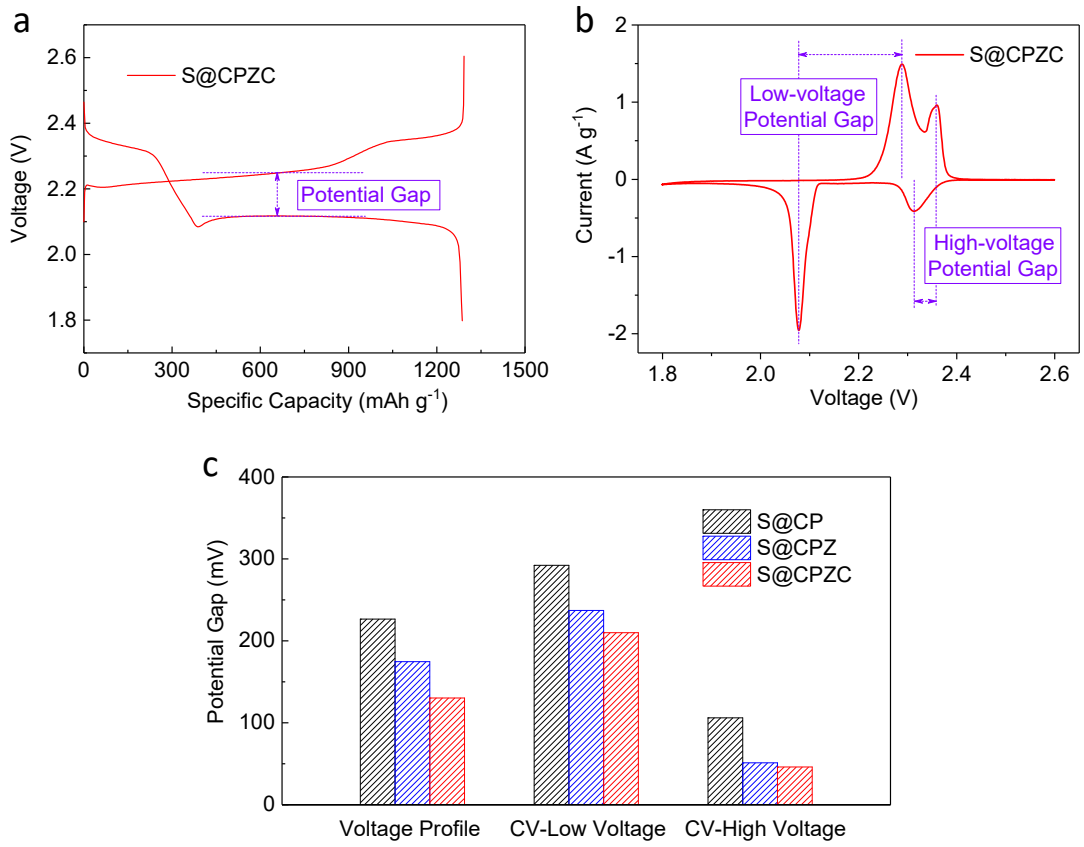

Figure S23. The potential gaps in voltage profile and CV curve for different sulfur electrodes. The potential gap in voltage profile is defined as the potential difference between charge and discharge curves at their respective half-capacity (a); the CV-Low Voltage and CV-High Voltage refer to the potential gaps of the sulfur redox pairs at lower and higher potentials respectively (b).

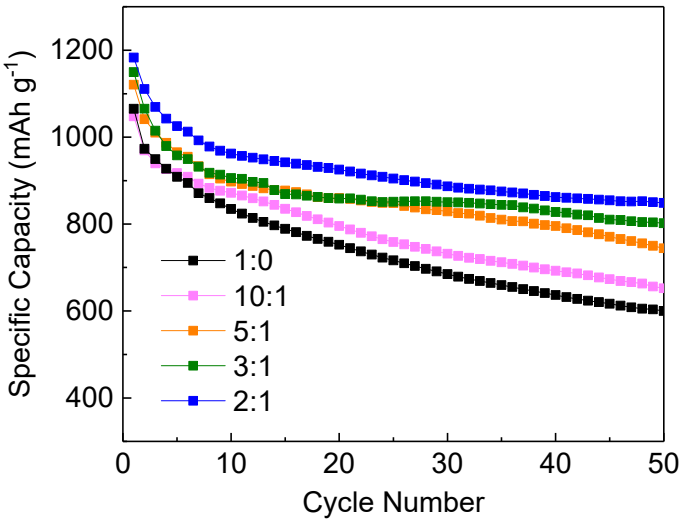

Figure S24. Cycling performances of S@CPZ electrodes with different PAN to ZIF ratios at C/5 rate.

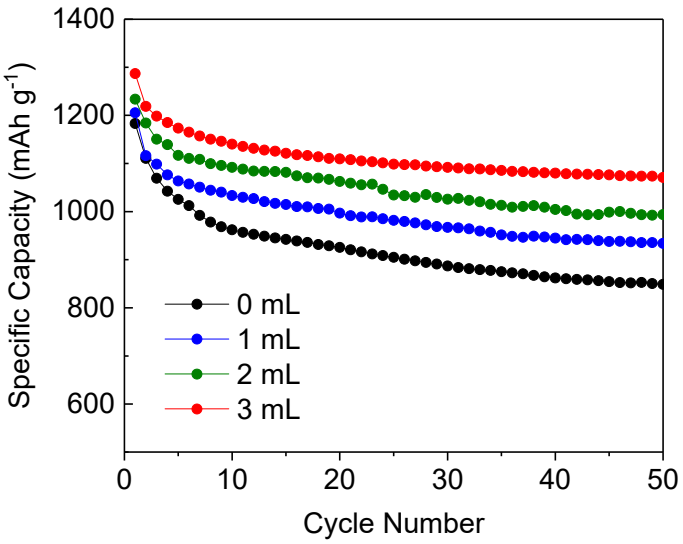

Figure S25. Cycling performances of S@CPZC electrodes with different EDA usages at C/5 rate.

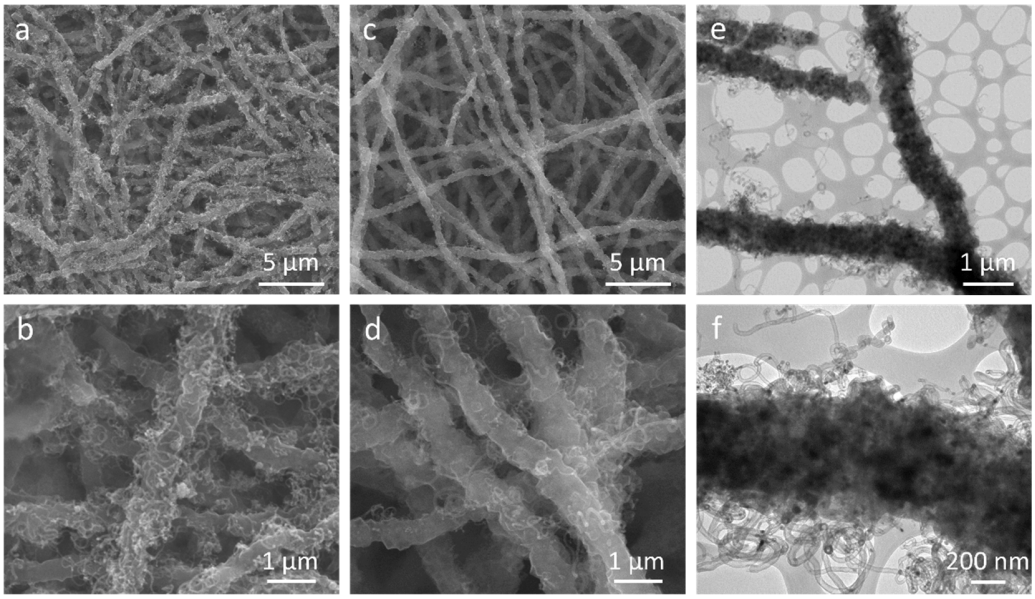

Figure S26. (a, b) SEM images of the cycled S@CPZC electrode; (c,d) SEM and (e, f) TEM images of S@CPZC after washing by THF and CS_2 to remove the sulfur species.

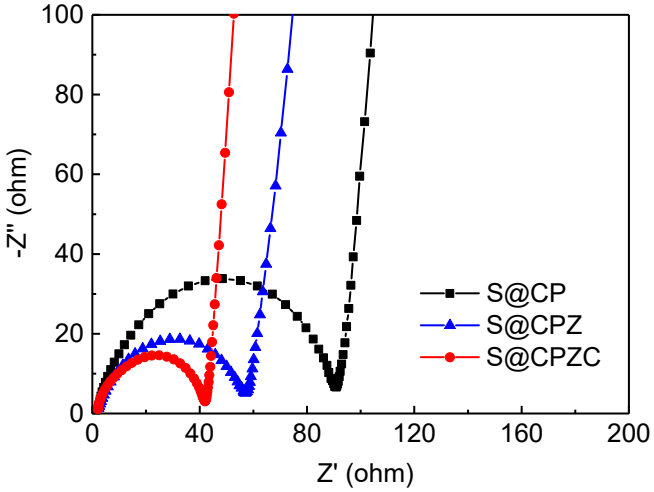

Figure S27. EIS spectra of different sulfur electrodes.

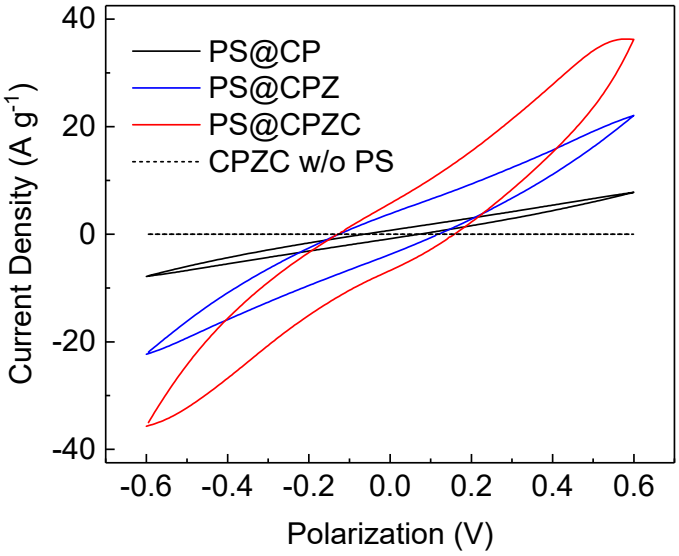

Figure S28. CV curves of different polysulfide (PS)-based electrodes in symmetrical cells.

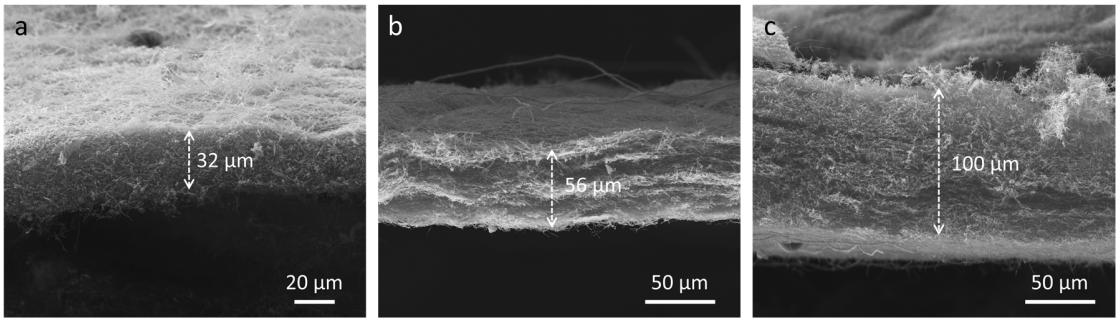

Figure S29. SEM images of thicker S@CPZC electrodes for higher sulfur loading of 2.8 (a), 5.1 (b), and 9.2 mg cm^{-2} (c).

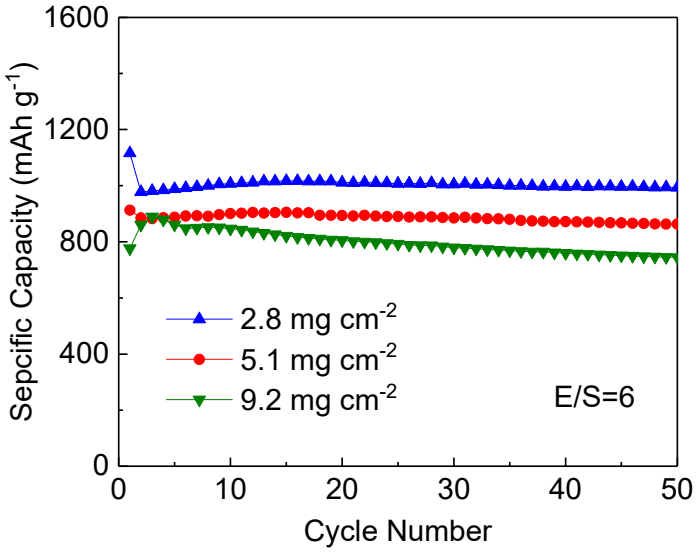

Figure S30. Specific capacities of S@CPZC electrodes under raised sulfur loading at C/5 rate.

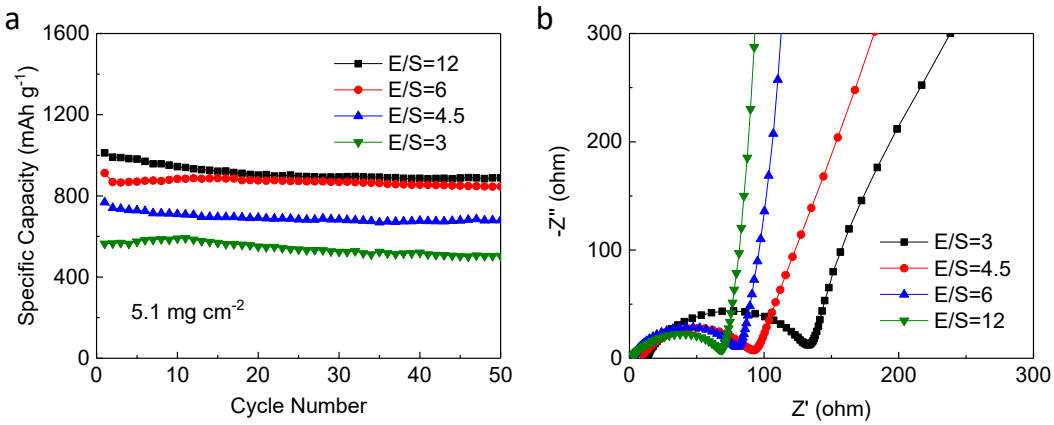

Figure S31. Specific capacities at C/5 rate (a) and EIS spectra (b) of S@CPZC electrode with different E/S ratios under sulfur loading of 5.1 mg cm^{-2}.

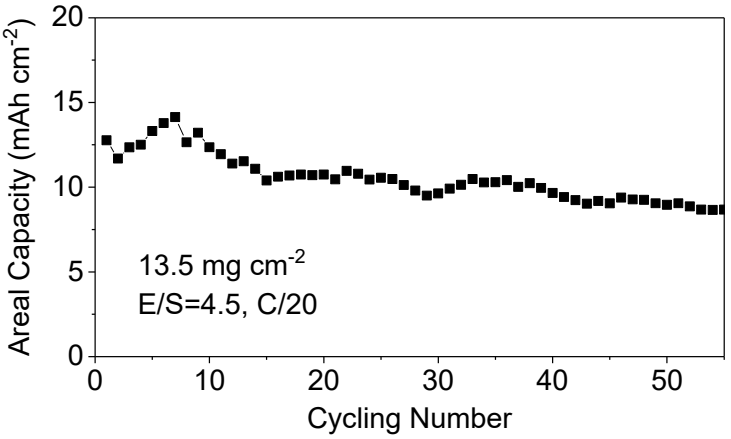

Figure S32. Cycling performance of S@CPZC electrode under high sulfur loading of 13.5 mg cm^{-2} and low E/S ratio of 4.5 at C/20 rate.

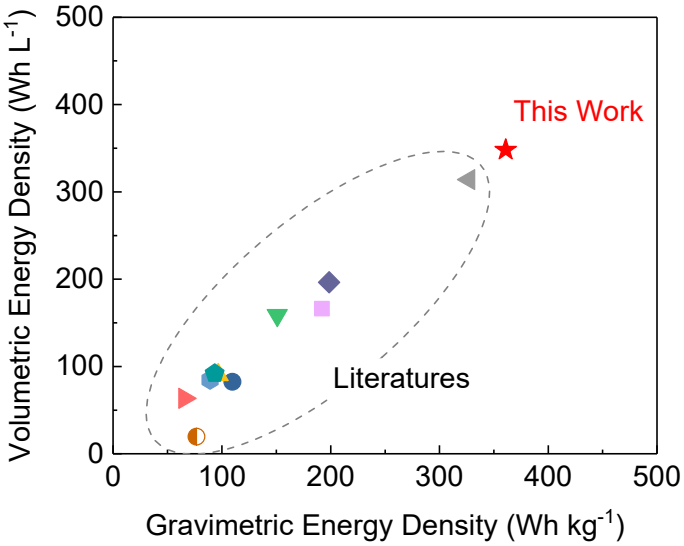

Figure S33. Energy density comparison between the Li-S batteries based on S@CPZC electrode and those with other fibrous sulfur electrodes in recent publications (details in Table S2).

Table S1. Performance comparison between S@CPZC electrode and the very recently published fibrous sulfur electrodes

Sulfur Electrode	Cyclability			Rate Capability		Ref.
	Rate (C)	Cycles	Capacity (mAh g^{-1})	Rate (C)	Capacity (mAh g^{-1})	
S@CNF	0.2 C	200	660	2 C	570	[4]
S@SNHCSs	0.2 C	50	685	2 C	688	[5]
S@TiO_2/G/NPCFs	1 C	500	618	5 C	668	[6]
S@NCFF	1 C	300	574	2 C	876	[7]
S@f-CMWF	0.24 C	450	859	2.4 C	430	[8]
S@NPCFs	5 C	500	427	5 C	540	[9]
S@HCF	2 C	500	620	4 C	860	[10]
S@HPCNF	0.5 C	300	700	0.5 C	800	[11]
S@CO_2-CNT	0.5 C	300	430	5 C	460	[12]
S@CNF/rGO	1 C	500	457	2 C	581	[13]
S@MVN@C NWs	1 C	200	636	10 C	543	[14]
S@CNTF	0.2 C	1000	713	3.2 C	507	[15]
S@rGO/CNT	0.1 C	100	416	0.5 C	313	[16]
S@GO-CTA-CNT	0.26 C	300	557	0.26 C	827	[17]
S@P-CNFs	1 C	200	720	2 C	670	[18]
S@ROGNT	1 C	500	492	2 C	605	[19]
S@ICFs/rGO	0.2 C	200	892	0.5 C	812	[20]
S@SWCNT/PEDOT	0.5 C	250	550	2 C	500	[21]
S@CPZC	**1 C**	**2000**	**712**	**10 C**	**623**	**This work**

Table S2. The performance comparison between S@CPZC and representative sulfur electrodes with different morphologies.

Electrode Morphology	Cyclability			Rate Capability		Ref.
	Rate (C)	Cycles	Capacity (mAh g^{-1})	Rate (C)	Capacity (mAh g^{-1})	
Yolk-shell carbon spheres	0.2 C	500	909	5 C	510	[22]
MnO_2@Carbon hollow nanoboxes	1.8 C	200	503	2.4 C	496	[23]
Co-graphitic carbon nanocages	0.5 C	500	833	2 C	387	[24]
Co-carbon polyhedrons@rGO	0.18 C	300	949	3 C	497	[25]
"Sea Urchin"-like carbon superstructure	1 C	1500	570	2 C	775	[26]
Bamboo-like CNT@yolk-shell carbon spheres	1 C	400	700	2 C	752	[27]
Porous carbon rods	1 C	300	700	5 C	646	[28]
Highly crumpled N-graphene sheets	0.5 C	300	920	1 C	950	[29]
Pyrrole-modified graphene foam	0.5 C	100	798	5 C	300	[30]
3D coral-like N-S co-doped carbon	2 C	250	621	10 C	693	[31]
Hollow carbon foam	0.1 C	100	654	0.5 C	524	[32]
Amino-graphene@ multichannel carbon nanofiber	0.2 C	200	950	2 C	363	[33]
Honeycomb-like mesoporous carbon nanosheets	0.5 C	500	506	2 C	580	[34]
Hierarchical porous carbon	1 C	300	809	5 C	470	[35]
Stringed "tube on cube"	**1C**	**2000**	**712**	**10 C**	**623**	**This work**

Table S3. Comparison between S@CPZC electrode and the high-sulfur-loading fibrous electrodes in recent publications

Sulfur Electrode	Loading (mg cm^{-2})	Thickness (μm)	Areal Capacity (mAh cm^{-2})	E/S ratio (mL g^{-1})	Gravimetric Energy Density (Wh kg^{-1})	Volumetric Energy Density (Wh L^{-1})	Ref.
S@NG-CNT	4.7	160	5.17	10	191.9	166.4	[36]
S@PCNFs	12	1020	13.5	20	109.7	82.5	[37]
S@3D-CNT	19.1	200	19.3	-	-	-	[38]
S@CNF@SWCNT	16	400	12.3	15	96.6	90.3	[39]
S@NCF/RGO	8.8	30	6.6	9	150.9	158.8	[40]
S@MWCNT	3.1	70	3.56	9.5	198.6	196.4	[41]
S@CF	2.32	36	3.75	8.7	327.0	314.1	[42]
S@CNT/NFC	8.1	210	8	30	65.7	63.6	[43]
S@PCF/VN	8.1	-	10.61	20	127.4	-	[44]
S@CNF	2.74	-	2.7	15	126.4	-	[4]
S@SN-HCSs	2.5	68.5	3.5	32	89.2	84.7	[5]
S@TiO_2/G/NPCFs	4.8	-	3.9	-	-	-	[6]
S@NCFF	3	2000	2.4	20	76.7	19.7	[7]
S@HPCNF	12.1	300	11.3	-	-	-	[11]
S@CNF/rGO	20.3	290	15.5	15.6	93.4	92.0	[13]
S@MVN@C NWs	9.7	-	7.1	-	-	-	[14]
S@CNTF	7.1	-	9	11	210.5	-	[15]
S@GO-CTA-CNT	11.1	-	12.5	4	419.8	-	[17]
S@G-HPC	3.6	-	4.26	11	196.8	-	[45]
S@CPZC	**13.5**	**160**	**14.2**	**4.5**	**360.9**	**348.1**	**This work**

Note: The energy densities are calculated at a system level covering the mass and volume of sulfur electrode, electrolyte, and lithium anode. Several assumptions were established in purpose of easier calculation as well as comparison: i) the density of electrolyte equals 1 g mL^{-1}; ii) nominal voltage of the batteries equals 2.15 V; iii) the lithium excess is 50%; iv) the total volume of the system sums up the volume of the components without regarding to the sparing space by electrolyte infiltration in porous structure.

Reference

1 H. L. Pan, X. L. Wei, W. A. Henderson, Y. Y. Shao, J. Z. Chen, P. Bhattacharya, J. Xiao and J. Liu, *Adv. Energy Mater.*, 2015, **5**, 1500113.
2 M. Cuisinier, C. Hart, M. Balasubramanian, A. Garsuch and L. F. Nazar, *Adv. Energy Mater.*, 2015, **5**, 1401801.
3 Q. Zou and Y. C. Lu, *J. Phys. Chem. Lett.*, 2016, **7**, 1518-1525.
4 S. Q. Li, J. Warzywoda, S. Wang, G. F. Ren and Z. Y. Fan, *Carbon*, 2017, **124**, 212-218.
5 D. Yang, W. Ni, J. L. Cheng, Z. P. Wang, T. Wang, Q. Guan, Y. Zhang, H. Wu, X. D. Li and B. Wang, *Appl. Surf. Sci.*, 2017, **413**, 209-218.
6 X. Song, T. Gao, S. Q. Wang, Y. Bao, G. P. Chen, L. X. Ding and H. H. Wang, *J. Power Sources*, 2017, **356**, 172-180.
7 W. Ren, W. Ma, S. Zhang and B. Tang, *Chem. Eng. J.*, 2018, **341**, 441-449.
8 C. Luo, H. L. Zhu, W. Luo, F. Shen, X. L. Fan, J. Q. Dai, Y. J. Liang, C. S. Wang and L. B. Hu, *ACS Appl. Mater. Inter.*, 2017, **9**, 14801-14807.
9 X. Song, S. Q. Wang, Y. Bao, G. X. Liu, W. P. Sun, L. X. Ding, H. K. Liu and H. H. Wang, *J. Mater. Chem. A*, 2017, **5**, 6832-6839.
10 X. Q. Zhang, B. He, W. C. Li and A. H. Lu, *Nano Research*, 2018, **11**, 1238-1246.
11 X. H. Zhao, M. Kim, Y. Liu, H. J. Ahn, K. W. Kim, K. K. Cho and J. H. Ahn, *Carbon*, 2018, **128**, 138-146.
12 D. Wang, K. Wang, H. Wu, Y. Luo, L. Sun, Y. Zhao, J. Wang, L. Jia, K. Jiang, Q. Li, S. Fan and J. Wang, *Carbon*, 2018, **132**, 370-379.
13 S. Han, X. Pu, X. Li, M. Liu, M. Li, N. Feng, S. Dou and W. Hu, *Electrochim. Acta*, 2017, **241**, 406-413.
14 X. X. Li, K. Ding, B. Gao, Q. W. Li, Y. Y. Li, J. J. Fu, X. M. Zhang, P. K. Chu and K. F. Huo, *Nano Energy*, 2017, **40**, 655-662.
15 R. Ummethala, M. Fritzsche, T. Jaumann, J. Balach, S. Oswald, R. Nowak, N. Sobczak, I. Kaban, M. H. Rummeli and L. Giebeler, *Energy Storage Materials*, 2018, **10**, 206-215.
16 W. G. Chong, J. Q. Huang, Z. L. Xu, X. Y. Qin, X. Y. Wang and J. K. Kim, *Adv. Funct. Mater.*, 2017, **27**, 1604815.
17 Y. Hwa, H. K. Seo, J. M. Yuk and E. J. Cairns, *Nano Lett.*, 2017, **17**, 7086-7094.
18 Y. Zhang, P. Wang, H. Tan, X. Fan and K. Huang, *J. Electrochem. Soc.*, 2018, **165**, A741-A745.
19 K. Chen, J. Cao, Q. Q. Lu, Q. R. Wang, M. J. Yao, M. M. Han, Z. Q. Niu and J. Chen, *Nano Research*, 2018, **11**, 1345-1357.
20 F. Wu, Y. S. Ye, J. Q. Huang, T. Zhao, J. Qian, Y. Y. Zhao, L. Li, L. Wei, R. Luo, Y. X. Huang, Y. Xing and R. J. Chen, *ACS Nano*, 2017, **11**, 4694-4702.
21 M. Zhang, Q. H. Meng, A. Ahmad, L. J. Mao, W. Yan and Z. X. Wei, *J. Mater. Chem. A*, 2017, **5**, 17647-17652.
22 J. Xu, H. B. Fan, D. W. Su and G. X. Wang, *J. Alloys Compd.*, 2018, **747**, 283-292.
23 S. Rehman, T. Y. Tang, Z. Ali, X. X. Huang and Y. L. Hou, *Small*, 2017, **13**, 1700087.
24 D. J. Xiao, Q. Li, H. F. Zhang, Y. Y. Ma, C. X. Lu, C. M. Chen, Y. D. Liu and S. X. Yuan, *J. Mater. Chem. A*, 2017, **5**, 24901-24908.
25 Z. Q. Li, C. X. Li, X. L. Ge, J. Y. Ma, Z. W. Zhang, Q. Li, C. X. Wang and L. W. Yin, *Nano Energy*, 2016, **23**, 15-26.

26 T. Chen, B. R. Cheng, G. Y. Zhu, R. P. Chen, Y. Hu, L. B. Ma, H. L. Lv, Y. R. Wang, J. Liang, Z. X. Tie, Z. Jin and J. Liu, *Nano Lett.*, 2017, **17**, 437-444.
27 S. K. Park, J. K. Lee and Y. C. Kang, *Adv. Funct. Mater.*, 2018, **28**, 1705264.
28 Z. M. Zheng, H. C. Guo, F. Pei, X. Zhang, X. Y. Chen, X. L. Fang, T. H. Wang and N. F. Zheng, *Adv. Funct. Mater.*, 2016, **26**, 8952-8959.
29 J. X. Song, Z. X. Yu, M. L. Gordin and D. H. Wang, *Nano Lett.*, 2016, **16**, 864-870.
30 K. Zhang, K. Y. Xie, K. Yuan, W. Lu, S. T. Hu, W. Wei, M. H. Bai and C. Shen, *J. Mater. Chem. A*, 2017, **5**, 7309-7315.
31 F. Wu, J. Li, Y. F. Tian, Y. F. Su, J. Wang, W. Yang, N. Li, S. Chen and L. Y. Bao, *Sci. Rep.*, 2015, **5**, 13340.
32 Y. B. An, Q. Z. Zhu, L. F. Hu, S. K. Yu, Q. Zhao and B. Xu, *J. Mater. Chem. A*, 2016, **4**, 15605-15611.
33 Z. Li, J. T. Zhang, Y. M. Chen, J. Li and X. W. Lou, *Nat. Commun.*, 2015, **6**, 8850
34 S. K. Park, J. Lee, T. Hwang, B. Jang and Y. Piao, *ACS Appl. Mater. Inter.*, 2017, **9**, 2430-2438.
35 G. R. Li, W. L. Cai, B. H. Liu and Z. P. Li, *J. Power Sources*, 2015, **294**, 187-192.
36 P. Y. Zhai, J. Q. Huang, L. Zhu, J. L. Shi, W. Zhu and Q. Zhang, *Carbon*, 2017, **111**, 493-501.
37 Y. Z. Zhang, Z. Zhang, S. Liu, G. R. Li and X. P. Gao, *ACS Appl. Mater. Inter.*, 2018, **10**, 8749-8757.
38 M. Y. Li, R. Carter, A. Douglas, L. Oakes and C. L. Pint, *ACS Nano*, 2017, **11**, 4877-4884.
39 C. H. Chang, S. H. Chung and A. Manthiram, *Mater. Horiz.*, 2017, **4**, 249-258.
40 M. W. Xiang, L. Yang, Y. F. Zheng, J. Huang, P. Jing, H. Wu, Y. Zhang and H. Liu, *J. Mater. Chem. A*, 2017, **5**, 18020-18028.
41 J.-Y. Hwang, H. M. Kim and Y.-K. Sun, *J. Electrochem. Soc.*, 2017, **165**, A5006-A5013.
42 H. Pan, J. Chen, R. Cao, V. Murugesan, N. N. Rajput, K. S. Han, K. Persson, L. Estevez, M. H. Engelhard, J.-G. Zhang, K. T. Mueller, Y. Cui, Y. Shao and J. Liu, *Nat. Energy*, 2017, **2**, 813-820.
43 M. Yu, J. Ma, M. Xie, H. Song, F. Tian, S. Xu, Y. Zhou, B. Li, D. Wu, H. Qiu and R. Wang, *Adv. Energy Mater.*, 2017, **7**, 1602347.
44 Y. Zhong, D. Chao, S. Deng, J. Zhan, R. Fang, Y. Xia, Y. Wang, X. Wang, X. Xia and J. Tu, *Adv. Funct. Mater.*, 2018, 1706391.
45 W. Deng, X. F. Zhou, Q. L. Fang and Z. P. Liu, *J. Mater. Chem. A*, 2017, **5**, 13674-13682.